1 **Model for heat and mass transport during cooking of cod loin in a convection oven**

2 Marthe J. Blikra[1, 2]*, Dagbjørn Skipnes[1] & Aberham H. Feyissa[2]

3

4 1. Nofima AS, Postbox 8034, NO-4068 Stavanger, Norway

5 2. DTU Food Production Engineering, Sølofts Plads, Building 227, 2800 Kgs Lyngby, Denmark

6 * Corresponding author. E-mail: marthe.blikra@nofima.no

7    Abbreviations: FEM - Finite element method; WHC - Water holding capacity

# 1   Introduction

9    Cooking of cod in a convection oven is a popular process, especially in the industry and the hotels,
10   restaurants, and catering market. During cooking, several changes occur in the muscle which affect the
11   eating quality of cod. Cod consists mainly of protein (~20 %) and water (~80 %), and one hypothesis is
12   that the changes during convective heating can be regarded mainly as consequences of protein
13   denaturation and moisture migration.

14   During cooking of cod, the collagens, which in the native state "bind" the myotome muscle sheets of the
15   fish together, denature first. The amounts of collagen are very small compared to the other proteins, so
16   it is usually not possible to detect denaturation of collagen when analyzing the denaturation peaks of
17   whole muscle. Collagen isolated from skin and bone of Pacific and Atlantic cod, respectively, showed
18   denaturation around 14-16 °C (Sun, Li, Song, Si, & Hou, 2017; Żelechowska, Sadowska, & Turk, 2010),
19   however higher denaturation values have also been reported (Hastings, Rodger, Park, Matthews, &
20   Anderson, 1985; Shu, Ren, Ao, Qi, & Zhang, 2017). Denaturation of collagens may lead to separation of
21   the myotome sheets, referred to as flaking. The majority of muscle protein is made up of the fibrillary
22   proteins myosin and actin. In cod, the myosin part of the myofibrillar proteins denature at 38.4-44 °C
23   (Skipnes, Van der Plancken, Van Loey, & Hendrickx, 2008). This change is correlated with whitening and
24   softening of the muscle (Ovissipour, Rasco, Tang, & Sablani, 2017). Sarcoplasmic proteins, which
25   constitute the soluble proteins of the sarcolemma (Tornberg, 2005), denature at 57.3-69.5 °C (Skipnes et
26   al., 2008). These protein solubilize in the liquid fraction of the fish, are exudated with water loss (Shibata-
27   Ishiwatari, Fukuoka, & Sakai, 2015), aggregate and contribute to the white color of the cook loss. If
28   heating is prolonged, the actin part of the myofibrillar proteins denature around 73.8-76.1 °C (Poulter,
29   Ledward, Godber, Hall, & Rowlands, 1985; Skipnes et al., 2008). This change is correlated with
30   toughening of the structure and increased hardness (Ovissipour et al. 2017). The extent of protein
31   denaturation depend on the amount of heat the sample is subjected to (i.e. temperature and exposure
32   time), as well as the history of the specimen (eg. freezing and temperature abuse during storage;
33   Hastings et al., 1985; Matos, Silva, Tiago, Aureliano, Dinis, & Dias, 2011; Poulter et al., 1985). In meat,
34   changes in the availability of water in the muscle tissue, as measured by NMR, correlated well with
35   protein denaturation temperatures (Bertram, Wu, van den Berg, & Andersen, 2006; Micklander, Peshlov,
36   Purslow, & Engelsen, 2002). For cod, there is a loss of juiciness, measured as water holding capacity
37   (WHC), for each major group of denatured proteins (Skipnes, Johnsen, Skåra, Sivertsvik, & Lekang, 2011),
38   which supports the claim that protein denaturation is correlated with moisture migration. Heat-induced
39   shrinkage of muscle, which is also associated with protein denaturation (Tornberg, 2005), may exert a
40   mechanical force on the tissue (van der Sman, 2007). The mechanical force may in turn contribute to
41   expulsion of free water and water-soluble compounds as cook loss. However, the mechanism and cause–
42   and–effect relationship of shrinkage and cook loss has not yet been firmly established. In addition to
43   expelled liquid, evaporation leading to surface drying will be an important process for water loss during
44   convection oven cooking at low relative humidity.

45   To minimize the weight loss and control the heat dependent quality changes, the cooking process can be
46   optimized using mathematical modeling of heat and mass transfer. Several studies of heat transfer
47   during cooking of fish were found in the literature, but none were coupled to mass transfer. In the
48   physics based studies, Fourier's law of conduction was used to model heat transfer in the product.

49    Convective boundary conditions were given by Newton's law of cooling, and, when relevant, in
50    combination with other modes of heat transfer, such as thermal radiation. The available publications
51    focusing on heat transfer in fish during heating consider steaming, immersion in water, and autoclaving
52    of vacuum-packed product. Models where cooking of cod was considered were used to confirm
53    measurements of thermal load and end-point temperature as performed by IR measurements (Stormo,
54    Sivertsen, Heia, & Skipnes, 2012), and to generate mild heat processing regimes that would inactivate
55    the bacteria on the surface of vacuumed-packed cod loins (Stormo, Skipnes, Sone, Skuland, Heia, &
56    Skåra, 2017). Other authors studied steaming of tuna, and used a 1-dimensional model to estimate the
57    core temperature, with good agreements between measured and simulated values (Bell, Farkas, Hale, &
58    Lanier, 2001).

59    To the best of our knowledge, no physics-based models for cooking of fish have been coupled with mass
60    transfer phenomena. However, models of coupled heat and mass transfer during cooking have been
61    established for other muscle-based foods. Datta (2007) suggested to use a porous media approach when
62    modeling mass transfer of muscle foods. Since the pores in muscle foods are small, Darcy's law can be
63    used to describe the velocity of the liquid, as formulated from conservation of momentum. van der Sman
64    (2007) applied Flory-Rehner theory to estimate the swelling pressure, which he stated as the driving
65    force in Darcy's law. The resulting swelling pressure was expressed as proportional to the difference
66    between the moisture content and the water holding capacity. He proposed that the details of molecular
67    processes (such as protein denaturation) was absorbed in the WHC term. The same approach has been
68    used in other studies when expressing the velocity of the liquid during cooking of meat and chicken (eg.
69    (Feyissa, Gernaey, & Adler-Nissen, 2013; Rabeler & Feyissa, 2018a)). An alternative approach is
70    considering the internal mass transfer as a pure diffusion process (Fick's law), i.e., by neglecting the
71    pressure driven transport of moisture in the muscle. However, this approach has been criticized since it
72    is not able to predict moisture transport inside the muscle (Feyissa et al., 2013; van der Sman, 2007).

73    There is a difference in the heating process between lean fish and meat during cooking. Some of this can
74    be ascribed to the difference in the muscle fiber macro-orientation in fish into myotomes, and a looser
75    overall structure in fish muscle due to less connective tissue compared to mammalian muscle tissue. In
76    addition, the muscle fibers of cod are much smaller than the muscle fibers of beef. Due to differences in
77    muscle structure, it is expected that some properties and mechanisms will differ. Therefore, the aim of
78    the present study was to determine the properties needed for prediction of heat and mass transfer
79    during cooking of cod, and develop and validate a numerical model for coupled heat and mass transport
80    during cooking of cod loin in a convection oven.

## 2  Model formulation

### 2.1  Process description

During cooking of lean fish muscle in a convection oven, heat is transferred from the hot air to the surface of the loin by convection and radiation, and from the baking plate by conduction (Figure 1). The heat is transported from the surface into the core of the loin by conduction and convection. Mass transport through the loin is driven by diffusion and convection. At the surface, mass is lost through evaporation and as exudate. In this study, it is assumed that all the liquid exudate evaporated from the fish surface. This can be argued for as follows: No visible amounts of cook loss was expelled to the baking tray during the first phase of heating. Only after cooking for 5–6 minutes, when the core temperature of our small samples was approaching 80 °C, bubbles of cook loss emerged from the sample surface (video recorded observations). For larger pieces of fish this does not hold true due to longer heating times and smaller surface area compared to the total volume, and this will therefore be dealt with in later research. Since the amount of fat in the cod was measured to <0.35 % (Section 3.8), no fat transport is a justified assumption. The energy that was consumed during denaturation of proteins, as measured previously using differential scanning calorimetry (eg. Skipnes et al., 2008) is very small compared to the energy transferred from the oven and was therefore neglected.

During cooking of normal sized cod loins, an unpredictable dimensional change was encountered, which made validating the heat and mass transfer model difficult. By reducing the sample size, the muscle was detached from its original macro-structure, and this resulted in a different kind of dimensional change, which occurred to a much lesser extent. The smaller samples were also much quicker to cook, which also contributed to limited dimensional change. This phenomena was therefore not taken into account in this study, but during cooking of cod loins with larger dimensions, this will have to be considered.

### 2.2 Geometry

The 3D model consisted of two domains: A rectangular cod sample and a baking tray (Figure 2). The cod sample was built with a surface area of 24x33 mm and height of 13 mm. During validation, the average sample dimensions used for each experiment was substituted. The fish sample had six boundary surfaces: The top, back, and right surfaces were external, and exposed to the oven air (Figure 2). The bottom surface was in direct contact with the baking tray. To reduce the computational burden, we took advantage of the symmetries of the geometry. Two symmetry planes (left and front) were used as shown in Figure 2, reducing both the length and the width of the studied sample to ½, and reducing the full sample volume to ¼. To yield the full rectangular geometry during computation, the solution was reflected along the lines of symmetry. Similar computational approaches taking advantage of symmetric boundary conditions were applied in other studies using the same software (Feyissa et al., 2013; Rabeler & Feyissa, 2018a). The core (1) and bottom surface (2) positions used for temperature validation are also shown in Figure 2.

The baking tray was constructed as a 1.4 mm thick 200x400 mm steel plate, upon which the cod sample was positioned in the middle. The baking plate was built with the same internal symmetry as the fish sample.

119 ## 2.3 Governing equations

120 ### 2.3.1 Heat transfer

121 The heat transfer in the fish (Equation 1a) and baking tray (Eq. 1b), is described by:

122 $$\rho c_p \left(\frac{\partial T}{\partial t}\right) + \nabla \cdot (-k\nabla T) + \rho_w c_{p,w} \boldsymbol{u_w} \, \nabla \cdot T = 0 \qquad (1a)$$

123 $$\rho c_p \left(\frac{\partial T}{\partial t}\right) + \nabla \cdot (-k\nabla T) = 0 \qquad (1b)$$

124 where he material properties are given by $\rho$, $c_p$, and $k$ – the density (kg/m³), specific heat (J/(kg K)), and
125 thermal conductivity (W/(m K)) of the materials (cod and baking tray), respectively. Similarly, $\rho_w$ and
126 $c_{p,w}$ are the thermophysical properties of the water transported within the fish sample, respectively. The
127 thermophysical properties used and the input parameters are given in Table 1. $\nabla$ is the three-
128 dimensional del operator i.e. partial derivative in x, y, and z direction ($\nabla = \partial/\partial x + \partial/\partial y + \partial/\partial z$). The
129 flow velocity of the liquid (m/s) is denoted by $u_w$, and $T$ is the temperature (K).

130 ### 2.3.2 Mass transfer

131 The mass transfer within the fish sample is based on the conservation mass (Bird, Stewart, & Lightfoot,
132 2002), and given by Eq. 2:

133 $$\frac{\partial c}{\partial t} + \boldsymbol{\nabla} \cdot (-D_w \nabla c + \boldsymbol{u_w} c) = 0 \qquad (2)$$

134 where $c$ is the moisture concentration (mol/m³) and $D_w$ is the moisture diffusion coefficient (m²/s) in the
135 sample. A porous media approach to determine the velocity inside the fish, where the driving force is
136 the pressure gradient in the sample (Datta, 2007). The velocity of the water inside the fish sample, $u_w$,
137 was described using Darcy's law (Eq. 3):

138 $$\boldsymbol{u_w} = -\frac{\kappa}{\mu_w} \nabla \boldsymbol{p} \qquad (3)$$

139 In Eq. 3, $\kappa$ is the permeability of cod (m²) and $\mu_w$ is the dynamic viscosity of water (Pa s). The swelling
140 pressure vector, $\boldsymbol{p}$, is proportional to the excess moisture concentration within the fish (Barrière &
141 Leibler, 2003; van der Sman, 2007), and is given by Eq. 4:

142 $$\boldsymbol{p} = G' \left(C - C_{eq}(T)\right) \qquad (4)$$

143 where $G'$ is the storage modulus of the cod as a function of temperature (kPa), which is given in Eq. 9
144 (see Section 4.4), and $C_{eq}(T)$ is the water holding capacity as a function of temperature, which is given in
145 Eq. 8 (see sections 4.3). $C$ denotes the mass fraction of water (kg/kg sample). Substituting Eq. 4 into Eq. 3
146 gives the following expression for the velocity of the liquid (Feyissa et al., 2013; Rabeler & Feyissa,
147 2018a):

148 $$\boldsymbol{u_w} = -\frac{\kappa \, G'}{\mu_w} \nabla \left(C - C_{eq}(T)\right) \qquad (5)$$

149    ## 2.4 Boundary conditions

150    ## 2.4.1 All external surfaces

151    ### *2.4.1.1 Heat transfer boundary conditions*

152    Combined convective and radiative flux boundary conditions were applied to all air-exposed external
153    surfaces (back, top, and right; Figure 2) of the fish sample and baking tray (Figure 2). The boundary
154    condition (Eq. 6) has a convective heat flux term given by a modified Newton's law of cooling (Feyissa et
155    al., 2013), and a radiative term given from the Stefan-Boltzmann law (Isleroglu & Kaymak-Ertekin, 2016):

156    $$-\boldsymbol{n} \cdot (-k\nabla T) = (1 - f_h)\big( h_c(T_{oven} - T_s) + \varepsilon\sigma\big(T_{wall}^4 - T_s^4\big) \big) \qquad (6)$$

157    where $h_c$ is the convective heat transfer coefficient (W/(m² K)), $T_{oven}$ is the measured average
158    temperature of the oven (K), and $T_s$ is the surface temperature (K). $f_h$ is a step function turning the heat
159    transfer off when the surface temperature approaches 100 °C (Feyissa et al., 2013). For the radiative part
160    of the equation, $\varepsilon$ *is* the measured emissivity of the oven at room temperature (-), $\sigma$ is Stefan
161    Boltzmann's constant (W/(m² K⁴)), and $T_{wall}$ is the wall temperature in the oven (K).

162    ### *2.4.1.2 Mass transfer boundary conditions*

163    The mass transfer boundary condition at the fish sample was applied to all external surfaces (back, top,
164    and right; Figure 2). The evaporative flux was modeled as described by Feyissa et al. (2013), and is the
165    diffusive flux relative to the convective flux (Eq. 7):

166    $$-\boldsymbol{n} \cdot (-D_w\nabla c) = -f_{evap} \frac{h_{total}(T_{oven} - T_s)}{H_{evap}} \frac{C_s - C_{air}}{M_w} \qquad (7)$$

167    where $f_{evap}$ is the measured fraction of the internal energy used for evaporation (Eq. 10; Section 4.5).
168    The nominator, Newton's law of cooling, represents the energy needed for evaporation, and the
169    denominator is given by the latent heat of evaporation, $H_{evap}$. The concentration gradient, $C_s - C_{air}$,
170    accounts for the difference between the mass fraction of water at the surface of the sample ($C_s$) and the
171    mass fraction of water in the oven air as calculated from the relative humidity ($C_{air}$). The latter term is the
172    driving force of the equation. It is divided by the molecular weight of water, $M_w$, for conversion of units.

173    ## 2.4.2 Bottom surface

174    Conductive heat transfer (Eq. 1b) was applied from the baking tray to the bottom fish surface (Figure 2).
175    A no flux mass transfer condition was also applied.

176    ## 2.4.3 Internal surfaces

177    Along the internal boundaries of the sample, namely the left and front surfaces (Figure 2), symmetry
178    boundary conditions were assigned to yield a solution for each element in the full geometry (see Section
179    2.2). Symmetry was also applied along the internal surfaces of the baking tray.

180 ## 2.5 Model solution

181 The mathematical model was solved using the Finite Element Method (FEM) in the software COMSOL

182 Multiphysics® version 5.4.

183 All domains (fish sample and baking tray) were meshed using the free tetrahedral method. A free

184 tetrahedral distribution with 50 number of elements were used to increase the resolution along the

185 edges of the fish (Figure 3). For the remaining geometry, the predefined "finer" setting in COMSOL

186 Multiphysics was applied (maximum element size: 0.88 mm; minimum element size: 0.064 mm;

187 maximum element growth rate: 1.4; curvature factor: 0.4; resolution of narrow regions: 0.7).

# 3 Experimental methods

## 3.1 Raw material

Cod (*Gadus morhua*) from the Aquaculture research station in Tromsø was used. The fish was 2 years old, had an average weight of 3.75 kg, and was starved for 9 days before slaughter in December 2017. The fish was sacrificed by a blow to the head, followed by bleeding in seawater at 5.7–6.0 °C for 25 minutes. The fish was then put on ice until direct filleting and deskinning to a filet weight of 373±75.8 g, numbered, followed by drying lightly with a paper towel, weighting, photographing, individual packaging in plastic bags, before packaging into Styrofoam containers with ice and absorbent, and transportation overnight to our lab in Stavanger. The next morning the temperature in the boxes were still 0 °C, and the fish was put in a storage room at 0 °C to undergo *rigor mortis.* After 5 days, the filets were cut into 2–4 pieces of depending on the size of the filet. The cod pieces used for analysis in this study were quick frozen directly in a freezing chamber at -60°C, vacuum packed at 92.2 % vacuum to avoid thawing, and stored at -80 °C until analysis to maintain the freshness and avoid major changes in water state.

## 3.2 Validation experiments

### 3.2.1 Sample preparation

Cod loins were selected from -80 °C storage and placed in a -30 °C freezer overnight. The loins were allowed to warm at 0 °C for 30–90 minutes prior to cutting to form a smooth top and bottom surface using a meat slicer, while also cutting away any brown muscle, gaping, or blood stains. The samples were still frozen when cut, but at a temperature high enough not to force expulsion of exudate when cutting. From each loin, 2–3 rectangular specimen were cut using a 20x30 mm stencil. The exact dimensions of each sample was measured using a caliper, prior to thawing on an aluminum tray under plastic film at 0–2 °C over night. From each fish, the water content was gravimetrically determined to 77.3±0.62 % from 4.0±0.2 g of finely chopped sample.

### 3.2.2 Calibration of thermocouples

The temperature probes used were calibrated at 0 °C in equilibrated ice water, and 30, 60, 90, 120 and 150 °C in a LiquiCal-HM oil bath (Ellab Validation Solutions, Hillerød, Denmark) using a recently calibrated ETS20 (Ellab Validation Solutions, Hillerød, Denmark) as a standard.

### 3.2.3 Temperature measurements

For temperature measurements, 11 samples were used. Thermocouples (SSA-TF, Ellab Validation Solutions, ±0.2 °C) were inserted into the geometric core of the samples and put in a central position between the sample and baking tray, hence referred to as the "bottom surface", and 15 cm above the fish in the oven, referred to as the oven temperature. The samples were allowed to equilibrate under plastic film in room temperature for 1 hour, then heated one-at-a-time for 12 minutes in a Metos System Rational oven (MSCC 61, Kerava, Finland). Prior to analysis, the oven was pre-heated for a minimum of 45 minutes at 148.2±1.59 °C, with a fan speed of 3/5. The humidity of the oven was measured to 6–9 % during cooking. During experiments, the baking tray with the fish sample was placed in position 2 from the bottom (approx. 1/3 up), with direct exposure from the oven fan from one side.

### 3.2.4 Measurement of average mass loss

For measurements of average mass loss, 12 cod loins and two samples per loin were used. The 24 samples had heights of 12.8±1.22 mm (as measured after thawing), widths of 33.2±0.45 mm, and depths of 23.9±0.40 mm. After cutting, the samples were divided into three batches of 8, 7, and 9 specimen, respectively, according to height. The samples were heated individually using the same oven and set-up as described above, for 2–10 minutes. The heating time was evenly distributed according to the number of samples in the batch, to spread the effect of dimensional differences. Care was also taken to disperse samples from the same fish throughout the heating time range. The samples were equilibrated for 30–45 minutes prior to cooking to minimize temperature gradients within the fish. Before and after heating, the samples were weighed to 4 decimals on an analytical scale, prior to gravimetric analysis (18 h, 105 °C) of the remaining fraction of water. The measured temperature profiles were divided into two groups based on the height of the fish sample prior to cooking, and the average dimensions, initial temperatures and oven temperatures measured for each group was used for the simulations.

### 3.3 Water holding capacity

Prior to analysis, eight frozen pieces of cod loins were cut horizontally into thin slices with a meat slicer. Any brown muscle was carefully cut away, and the remaining muscle was finely chopped. The small pieces were distributed into sealed plastic bags and thawed over night at 0–2 °C. Analysis of water holding capacity (WHC) was performed the following two days, using the methodology described by Skipnes, Østby, & Hendrickx (2007), with some alterations. Briefly, 4.2±0.13 g of fish pieces were weighed into cooled, pre-weighed steel sample cups. The cups had an adjustable, central filter, making the fish sample closely situated to the top of the cup, and the expelled liquid was allowed to exit to the removable bottom. For analysis of cooked samples, the filled sample cup was isothermally heated in a water bath (GR150, Grant Instruments, Cambridge, UK) at 25, 30, 35, 40, 50, 70 and 90 °C for 10 minutes, before cooling in ice water for at least 5 minutes. The exudate was removed to determine the amount of cook loss, before centrifugation (Rotina 420R, Hettich, Tuttlingen, Germany) at 4 °C for 15 minutes at 528 g. The water holding capacity was determined as the remaining mass after centrifugation as a fraction of the original, raw mass. The gravimetrically determined (18 h, 105 °C) water content of each individual fish was used in the calculation.

### 3.4 Determination of storage modulus

Prior to analysis, five frozen pieces of cod were cut horizontally into 3 mm thick slices using a meat slicer. Circles of 30 mm were then cut from the slices using a sharp edged pipe, while avoiding any brown muscle and uneven areas. The discs were singly put in small plastic bags, vacuum packed at 92.2 % vacuum, and  stored at -80 °C until analysis. To avoid thawing of the samples, the preparation was performed in a chill room with circulating air at 0–2 °C.

A Discovery hybrid rheometer-2 from TA Instruments (New Castle, DE, USA) with a 20 mm cross-hatched parallel plate and temperature control connected to a heat exchanger (P/N 953260.901 TGA, TA Instruments) was used for the analysis. Fish samples were collected one–at–a–time from storage, thawed in ice water while still in the vacuum bag (<5 min), and put on the 0 °C Peltier plate. Amplitude sweeps were run at 1 Hz / 0.01–100 % strain at 25 °C, as well as 40, 60, and 80 °C after preheating for 10 and 60 minutes to ensure that strain in the linear viscoelastic region was applied in later testing. Temperature ramps were performed at 0.05 % strain, and 1.0 Hz frequency, from 0–100 °C, with a constant heating rate of 2.5 °C/min (n=9). Prior to all testing, a conditional step was included to lower

267  the geometry to 0.25±0.1 N axial force. A solvent trap was placed around the sample and geometry to
268  prevent heat loss and drying of the sample, and aluminum foil was placed around the solvent trap for
269  additional prevention of heat loss.

## 3.5 Evaluating the fraction of energy used for evaporation

271  Since water evaporates from the cook loss after it leaves the fish, the original amount of water leaving
272  the fish as cook loss was calculated from the original dry matter content of the cook loss (Section 3.5.1).
273  From this and the weight loss of the fish sample (Section 3.5.2), the weight loss due to evaporation was
274  determined. This value was used together with the core temperatures, heat capacity, sample mass, and
275  time between reaching the various core temperatures, to determine the fraction of energy used for
276  evaporation, as theoretically described by Feyissa et al. (2013).

### 3.5.1 Original dry matter content in cook loss

278  The original moisture content in the cook loss was determined by heating vacuum packed (92.2 %
279  vacuum) rectangular specimen (17x20x30 mm) of cod together with a 30 mm glass tube in a water bath
280  (GR150, Grant Instruments, Cambridge, UK). The glass tube was included to lead the liquid away from
281  the specimen, allowing for easier collection. The amount of dry matter in the cook loss was determined
282  gravimetrically, by weighting the cook loss into pre-weighed aluminum cups with a thin layer of pre-dried
283  sea sand (pro analysis, Merch KGaA, Darmstadt, Germany), and drying in a heating cabinet at 105 °C for
284  16-18 hours before weighting again (ISO 6496, 1999).

### 3.5.2 Measurement of evaporation

286  From four cod loins, three 16x20x30 mm samples per loin were cut as described in Section 3.2.1. One
287  sample per loin was used for each temperature. The samples were weighed in pre-weighed aluminum
288  cups with height 1–2 mm around the edge before and after heating. Mineral isolated thermocouples
289  (Testo, West Chester, PA, USA, ±1 °C) were inserted in the core position and centered between the
290  sample and the cup at the bottom. The samples were heated one-at-a-time in the oven as described in
291  Section 3.2.3 until a core temperature of 50, 70, or 90 °C was reached. After heating, the weight of the
292  samples and cook loss was recorded, before gravimetric determination of the fraction of water in the
293  cook loss accompanying each sample. The water concentration in the cook loss was determined to 90–92
294  %.

## 3.6 Estimation of the emissivity in the oven

296  The emissivity was estimated using an IR thermal camera (MobIR® M8, PAL/NTSC, 9V) from Wuhan
297  Guide Infrared (Wuhan, P. R. China). The camera was secured to a tripod 1 m from the oven wall. A triple
298  layer of black plastic was used to cover the oven door opening, and a hole just large enough for the
299  camera lens was cut out. The camera was then taped to the plastic around the opening, allowing no light
300  to escape into the oven. The relative humidity setting used was calculated from the wet and dry bulb
301  temperature in the oven. The emissivity setting in the camera was then changed until the temperature in
302  the oven as measured by the camera was in accordance with the temperature measured using the
303  calibrated thermocouples.

## 3.7 Determination of the heat transfer coefficient

The heat transfer coefficient was determined as described by Ghisalberti & Kondjoyan (1999) and
summarized by Skåra, et al. (2014), using the same aluminum cylinder (Ø=30 mm, h=30 mm) as
described. Thermocouples type K (PR Electronics Inc., San Diego, CA) were used for measurement of the
geometrical center of the cylinder. Prior to measurements, the accuracy was determined to ±0.37 °C
between 30-150 °C. The oven temperature was recorded using a high temperature thermocouple
(STC25012E700KT, Ellab Validation Solutions, Hillerød, Denmark) calibrated to an accuracy of ±0.2 °C.
The oven was pre-heated and allowed to equilibrate for 20-30 minutes prior to analysis, using the same
settings and an empty baking tray in the same position as described above (Section 3.2.3). The cylinder
was hanged centrally in the oven from a cooling rack, within 5–10 cm of the thermocouple, and within 2–
3 cm of the baking plate. Temperatures were recorded for 40 minutes (n=2), and the total surface,
radiative and convective heat transfer was determined using the lumped capacity method as described
by Isleroglu & Kaymak-Ertekin (2016).

## 3.8 Chemical analysis of fat

The amount of fat in the muscle was analyzed using ethyl acetate extraction (NS 9404, Nofima BioLab)
from a sample of 10.4±0.5 g from 6 fish loins, and reported as 0.298±0.0305 %.

## 3.9 Statistics

Statistical analysis was performed using Minitab® 18.1. One-way ANOVA with 95 % confidence interval
and Tukey post-hoc test was performed for analysis of significant difference. Analysis of outliers was
performed using Dixon's Q test with 0.05 % significance level. Analysis of linear correlation coefficients
($R^2$) was performed using Microsoft® Excel® 2013.

# 4 Results and discussion

## 4.1 Heat transfer prediction and validation

The developed model of heat transfer predicts the temperature at each point in space and time. As shown in Figure 4, the temperature distribution in a fish sample can be obtained at specific cooking times. After 1 minute, a gradient is forming throughout the fish, with the highest temperature on the surface and the lowest near the geometric core. After 4.5 minutes of cooking, the small (13.4x24.4x33.4 mm) piece of fish has already reached a temperature of 70 °C in the coldest spot.

The effect of the conductive heating from the baking tray to the fish can also be seen from the model prediction since the coldest spot is raised from the geometric core. In Figure 4, this is easiest to see after 3 minutes of cooking, when the temperature at the bottom surface is red and has surpassed 90 °C, whereas the temperature at the central top surface remains at the color orange under 80 °C. Thus, in the portrayed scenario, the conductive heating from the baking tray is quicker than the convective and radiative heating from the surrounding air.

The model prediction at the core and bottom surface positions (Figure 2) were compared to the measured data from the same positions, as seen in Figure 5. There is a generally good agreement between the measured and the predicted temperatures, and the curves show a similar tendency in slope and lag. For the core temperature prediction, the model is within 2 °C in the critical range between 40–80 °C. After 80 °C, the average measured core temperature rises somewhat quicker than the prediction. This is probably attributed to shrinkage in height during this region, which would lead to quicker heating of the sample.

The fit in the range 40–80 °C is made even better when including the geometry and parameters of the thermocouple in the model simulation (Figure 6). The thermocouple was modeled as a 40 mm long hollow stainless steel (316L) cylinder using the measured diameter and wall thickness of the electrode, 1.2 and 0.08 mm, respectively, with thermophysical properties from Kim (1975). The volume inside was assumed to have the same insulating properties as air. When the sample size is increased to 80x60x25 mm, which is a normal size for a cod loin, the effect of the thermocouple on the core temperature diminishes to under 0.8 °C. During cooking of samples of normal dimensions, the effect can therefore be neglected.

## 4.2 Mass transfer prediction and validation of average mass loss

The predicted moisture profile shows that there is a gradual drying of the sample surface, and a drying front is slowly moving inwards during cooking (Figure 7). According to our model, the change in the water profile in the central positions is very slow.

The predicted average mass fraction of water in the sample is very dependent on the relative humidity of the oven, since the evaporative (mass transfer) boundary condition is driven by the difference between the moisture concentration on the sample surface and the relative humidity of the oven air. Figure 8 shows the effect of raising the humidity of the oven on the predicted average evaporation rate. Increasing the humidity to 50 % reduces the evaporative weight loss after 4.5 minutes by 3.5 % compared to a relative humidity of 10 %. Like the figure shows, humidity can be an important parameter in process optimization to minimize the weight lost as evaporation.

364    In this study, mass transfer was only validated using average mass loss data. While this method has
365    limitations, including not showing the moisture profile within the sample during cooking, it is able to give
366    a gross overview of how the reality fits the prediction on a macro-scale. However, in order to truly
367    validate the mass transfer model, information about the distribution and movement of moisture during
368    cooking must be acquired.

369    Our measurements showed that during cooking of 12.8x33.2x23.9 mm samples, the mass fraction of
370    water decreased linearly from the initial 77.5 % until it reached 68.9±0.491 % after 10 minutes. For the
371    first 8.5 minutes of the process, there was good agreement between the measured and the predicted
372    water concentration in the samples (Figure 9). After cooking for 10 minutes, all measured data values
373    were below the model prediction, with 1.3 % between average measured and predicted values. During
374    the last stage of heating (8-10 min), cook loss was expelled from the sample surface in addition to
375    evaporation (video recorded observations). Since the mass transfer boundary condition only included
376    evaporation and not mass lost in liquid form as cook loss, the deviation can be accounted for in the
377    future by adding equations of cook loss to the model. This is especially important when predicting the
378    mass loss during cooking from larger samples.

379    ## 4.3 WHC
380    The water holding capacity (WHC) of the raw fish was measured to 81.3±0.822 % (Figure 10). From 25 to
381    40 °C, the WHC decreased until reaching a local minimum of 67.0±4.83 %, which is a similar trend to
382    what has been found previously for post-rigor fileted farmed cod (Skipnes et al., 2011). In this study,
383    consistently higher values were found throughout the temperature range for pre-rigor fileted fish than
384    was found for post-rigor fileted fish in the aforementioned study. This may be a consequence of
385    increased loss of free water during the *rigor mortis* stage when fileting prior to this biological process
386    (Kristoffersen, Vang, Larsen, & Olsen, 2007), leaving the fish with less water available for loss during
387    cooking and centrifugation. From 40 to 90 °C, there were no significant differences between the
388    measured temperature points. It therefore seems that the water holding capacity reached a plateau
389    after the proteins were denatured. The average value obtained after cooking at 40-90 °C was used as the
390    final value in the proposed equation. There were large standard deviations accompanying the data on
391    account of large biological differences between each fish. The low or high WHC behavior seen in each
392    fish specimen was consistent along the temperature range applied.

393    A function for the change in water holding capacity with temperature has previously been formulated by
394    van der Sman (2007). The experimental data found for farmed cod was fitted to this relation to give a
395    function for WHC of cod muscle (Eq. 8):

396    $$C_{eq}(T) = C_{eq,0} - \frac{a_1}{1+a_2\,exp(-a_3(T-T_\sigma))}$$    (8)

397    where $C_{eq,0}$ is the initial water holding capacity of raw sample, 0.82, $T$ is the temperature in °C, $T_\sigma$ is the
398    center of a logistic curve, 25 °C, and $a_1$, $a_2$, and $a_3$ are fitting parameters set to 0.12, 23.0, and 0.42 by
399    trial-and-error. It should be noted that the water holding capacity is specific to the raw material, and
400    affected by conditions before, during, and after sacrificing the fish. Especially, differences are expected
401    between wild and farmed cod (Rustad, 1992), between pre- and post rigor fileted cod, and as a
402    consequence of freezing regimes (Schubring, 2005). When differences in WHC is found, the parameters
403    of Eq. 8 should be adjusted accordingly.

404    ## 4.4 Rheological analysis

405    The rheological measurements (Figure 11) showed that the storage modulus ($G'$) of cod decreased
406    initially from 0–37 °C, before an increase between 50–75 °C, and eventually a plateau was reached after
407    heating to 80-100 °C. The change in G' as a function of temperature was fitted to a sigmoidal curve, as
408    outlined in Feyissa et al. (2013) for meat and in Rabeler & Feyissa (2018b) for chicken breast (Eq. 9):

409    $$G'(T) = G'_{max} + \frac{G'_{min} - G'_{max}}{1 + exp\left(\frac{T - g_1}{g_2}\right)}$$    (9)

410    where $G'_{max}$ is the mean maximum elastic modulus, 48.2±8.55 kPa, $G'_{min}$ is the lowest measured elastic
411    modulus, 14.2±3.20 kPa, T is the temperature (°C), and $g_1$ and $g_2$ are fitting patterns with values 64 and
412    5, respectively, determined by trial-and-error.

413    The data, especially after 70 °C, was accompanied by large standard deviations, which yields an
414    uncertainty for the equation. This is not unexpected, since measurements of cod texture have been
415    correlated with high standard deviations also previously, when using a compression test to measure
416    hardness (Skipnes et al., 2011). When statistically analyzing the storage modulus at critical points (0, 37,
417    and 76 °C), no correlation between sample height and storage modulus was found ($R^2$<0.28).

418    ## 4.5 Fraction of internal energy used for evaporation

419    The fraction of internal energy used for evaporation, calculated from the measured data and plotted
420    against the average core temperature of the time intervals used for the calculation (0–50 °C, 50–70 °C
421    and 70–90 °C), is shown in Figure 12. In the case of samples cooked from 0-50 °C, the fraction of internal
422    energy used for evaporation had already reached 0.19±0.05. For samples reaching a core temperature of
423    70 and 90 °C, the fraction increased to 0.78±0.02 and 0.86±0.01, respectively. The fitted sigmoidal
424    function describing the fraction of internal energy used for evaporation, $f_{evap}(T)$, is given by Eq. 10:

425    $$f_{evap}(T) = f_{max} + \frac{f_0 - f_{max}}{1 + exp\left(\frac{T - f_1}{f_2}\right)}$$    (10)

426    where $f_{max}$ is the maximum fraction of internal energy that can be used for evaporation, 1, which is
427    achieved at the boiling point of water, 100 °C. The fraction of evaporation at the freezing point, 0 °C,
428    given by $f_0$, has a value of 0. T is the surface temperature (°C) of the sample, and $f_1$ and $f_2$ are fitting
429    parameters with values 47 and 15, respectively, determined by trial-and-error and visual inspection of
430    the curves. In practice, this function gradually turns up the fraction of internal energy used for
431    evaporation at the surface.

## Conclusion

A comprehensive model of heat and mass transport during baking of small pieces of cod on a baking tray in a convection oven was formulated. The model showed the ability to predict the temperature and moisture concentration during cooking as functions of time and space. Empirical relations for storage modulus and water holding capacity of cod were developed, as well as a relation for the fraction of internal energy used for evaporation. The model does not consider dimensional change and expulsion of water as cook loss, which are processes of great importance when heating larger pieces of cod. In order to make a more general model with a larger specimen validity range, these processes will be considered in later studies. In addition, quality and safety parameters can be added, so that the model may assist industry and the hotels, restaurants, and catering businesses in process optimization to minimize the liquid loss and optimize quality, while maintaining safety.

## Acknowledgements

## References

447  References

448  Barrière, B., & Leibler, L. (2003). Kinetics of solvent absorption and permeation through a highly
449      swellable elastomeric network. *Journal of Polymer Science Part B: Polymer Physics, 41*(2), 166-
450      182.
451  Bell, J. W., Farkas, B. E., Hale, S. A., & Lanier, T. C. (2001). Effect of thermal treatment on moisture
452      transport during steam cooking of skipjack tuna (*Katsuwonas pelamis*). *Journal of Food Science,*
453      *66*(2), 307-313.
454  Bertram, H. C., Wu, Z., van den Berg, F., & Andersen, H. J. (2006). NMR relaxometry and differential
455      scanning calorimetry during meat cooking. *Meat Science, 74*(4), 684-689.
456  Bird, R. B., Stewart, W. E., & Lightfoot, E. N. (2002). *Transport phenomena* (2 ed.). New York: Wiley &
457      Sons, Inc.
458  Datta, A. K. (2006). Hydraulic permeability of food tissues. *International Journal of Food Properties, 9*(4),
459      767-780.
460  Datta, A. K. (2007). Porous media approaches to studying simultaneous heat and mass transfer in food
461      processes. I: Problem formulations. *Journal of Food Engineering, 80*(1), 80-95.
462  Feyissa, A. H., Gernaey, K. V., & Adler-Nissen, J. (2013). 3D modelling of coupled mass and heat transfer
463      of a convection-oven roasting process. *Meat Science, 93*(4), 810-820.
464  Ghisalberti, L., & Kondjoyan, A. (1999). Convective heat transfer coefficients between air flow and a short
465      cylinder. Effect of air velocity and turbulence. Effect of body shape, dimensions and position in
466      the flow. *Journal of Food Engineering, 42*(1), 33-44.
467  Hastings, R. J., Rodger, G. W., Park, R., Matthews, A. D., & Anderson, E. M. (1985). Differential scanning
468      calorimetry of fish muscle: The effect of processing and species variation. *Journal of Food*
469      *Science, 50*(2), 503-506.
470  Isleroglu, H., & Kaymak-Ertekin, F. (2016). Modelling of heat and mass transfer during cooking in steam-
471      assisted hybrid oven. *Journal of Food Engineering, 181*, 50-58.
472  ISO 6496 (1999). *Animal feeding stuff - Determination of moisture and other volatile matter content* (2
473      ed.). Geneve, Switzerland: International Organization for Standardization.
474  Kim, C. S. (1975). *Thermophysical properties of stainless steels. Report ANL-75-55*. Argonne, Illinois, USA:
475      Argonne National Laboratory.
476  Köckher & co (2019). *1.4301 (X5CrNi18-10)* [Internet]. Germany: Köckher & co. Accessed from
477      https://facts.kloeckner.de/werkstoffe/stahl/1-4301/
478  Kristoffersen, S., Vang, B., Larsen, R., & Olsen, R. L. (2007). Pre-rigor filleting and drip loss from fillets of
479      farmed Atlantic cod (Gadus morhua L.). *Aquaculture Research, 38*(16), 1721-1731.
480  Matos, E., Silva, T. S., Tiago, T., Aureliano, M., Dinis, M. T., & Dias, J. (2011). Effect of harvesting stress
481      and storage conditions on protein degradation in fillets of farmed gilthead seabream (*Sparus*
482      *aurata*): A differential scanning calorimetry study. *Food Chemistry, 126*(1), 270-276.
483  Micklander, E., Peshlov, B., Purslow, P. P., & Engelsen, S. B. (2002). NMR-cooking: Monitoring the
484      changes in meat during cooking by low-field ^{1}H-NMR. *Trends in Food Science & Technology, 13*(9-
485      10), 341-346.
486  Ovissipour, M., Rasco, B., Tang, J., & Sablani, S. (2017). Kinetics of protein degradation and physical
487      changes in thermally processed Atlantic salmon (*Salmo salar*). *Food and Bioprocess Technology,*
488      *10*(10), 1865-1882.
489  Poulter, R. G., Ledward, D. A., Godber, S., Hall, G., & Rowlands, B. (1985). Heat stability of fish muscle
490      proteins. *International Journal of Food Science and Technology, 20*(2), 203-217.
491  Rabeler, F., & Feyissa, A. H. (2018a). Modelling the transport phenomena and texture changes of chicken
492      breast meat during the roasting in a convective oven. *Journal of Food Engineering, 237*, 60-68.

493 Rabeler, F., & Feyissa, A. H. (2018b). Kinetic modeling of texture and color changes during thermal
494     treatment of chicken breast meat. *Food and Bioprocess Technology, 11*(8), 1495-1504.
495 Rustad, T. (1992). Muscle chemistry and the quality of wild and farmed cod. In H. H. Huss, M. Jacobsen &
496     J. Liston (Eds.), *Quality assurance in the fish industry*,  (pp. 19-27). London: Elsevier Science
497     Publishers.
498 Shibata-Ishiwatari, N., Fukuoka, M., & Sakai, N. (2015). Changes in the viscosity of expressible water in
499     meat during heating: Description based on the denaturation kinetics of water-soluble proteins.
500     *Food Science and Technology Research, 21*(4), 525-530.
501 Shu, Y., Ren, H., Ao, R., Qi, W., & Zhang, Z. (2017). Comparison of physical and chemical characteristics of
502     collagen from the skin of cod (*Gadus macrocephaius*). *Genetics and Molecular Research*, 16(2).
503 Singh, R. P., & Heldman, D. R. (2014). Appendix A.4 Physical properties of water and air. In S. L. Taylor
504     (Ed.), *Introduction to Food Engineering* (5 ed.). London, England: Elsevier, Academic Press.
505 Schubring, R. (2005). Changes in texture, water holding capacity, colour and thermal stability of frozen
506     cod (*Gadus morhua*) fillets: Effect of frozen storage temperature. *Deutsche Lebensmittel-*
507     *Rundschau*, 101(11), 484-493.
508 Skåra, T., Stormo, S. K., Skipnes, D., Kondjoyan, A., Sivertsen, A., Gins, G., Van Derlinden, E., Valdramidis,
509     V. P., & Van Impe, J. F. M. (2014). Estimation of surface temperature and thermal load in short-
510     time heat treatment of surimi through reflectance spectroscopy and heat transfer modeling.
511     *Journal of Food Engineering, 120*, 75-80.
512 Skipnes, D., Johnsen, S. O., Skåra, T., Sivertsvik, M., & Lekang, O. (2011). Optimization of heat processing
513     of farmed Atlantic cod (*Gadus morhua*) muscle with respect to cook loss, water holding capacity,
514     color, and texture. *Journal of Aquatic Food Product Technology, 20*(3), 331-340.
515 Skipnes, D., Østby, M. L., & Hendrickx, M. E. (2007). A method for characterising cook loss and water
516     holding capacity in heat treated cod (*Gadus morhua*) muscle. *Journal of Food Engineering, 80*(4),
517     1078-1085.
518 Skipnes, D., Van der Plancken, I., Van Loey, A., & Hendrickx, M. E. (2008). Kinetics of heat denaturation of
519     proteins from farmed Atlantic cod (*Gadus morhua*). *Journal of Food Engineering, 85*(1), 51-58.
520 Stormo, S. K., Sivertsen, A. H., Heia, K., & Skipnes, D. (2012). Endpoint temperature of heat-treated
521     surimi can be measured by visible spectroscopy. *Food Control, 26*(1), 92-97.
522 Stormo, S. K., Skipnes, D., Sone, I., Skuland, A., Heia, K., & Skåra, T. (2017). Modeling-assisted minimal
523     heat processing of Atlantic cod (*Gadus morhua*). *Journal of Food Process Engineering, 40*(6),
524     e12555.
525 Sun, L., Li, B., Song, W., Si, L., & Hou, H. (2017). Characterization of Pacific cod (*Gadus macrocephalus*)
526     skin collagen and fabrication of collagen sponge as a good biocompatible biomedical material.
527     *Process Biochemistry*, 63, 229-235.
528 Tornberg, E. (2005). Effects of heat on meat proteins - Implications on structure and quality of meat
529     products. *Meat Science, 70*(3), 493-508.
530 Valle, F. D., & Nickerson, J. (1968). Salting and drying fish. 3. Diffusion of water. *Journal of Food Science,*
531     *33*(5), 499-503.
532 van der Sman, R. G. M. (2007). Soft condensed matter perspective on moisture transport in cooking
533     meat. *American Institute of Chemical Engineers, 53*(11), 2986-2995.
534 Vestergaard, C., Risum, J., & Adler-Nissen, J. (2005). [23]Na-MRI quantification of sodium and water
535     mobility in pork during brine curing. *Meat Science, 69*(4), 663-672.
536 Żelechowska, E., Sadowska, M., & Turk, M. (2010). Isolation and some properties of collagen from the
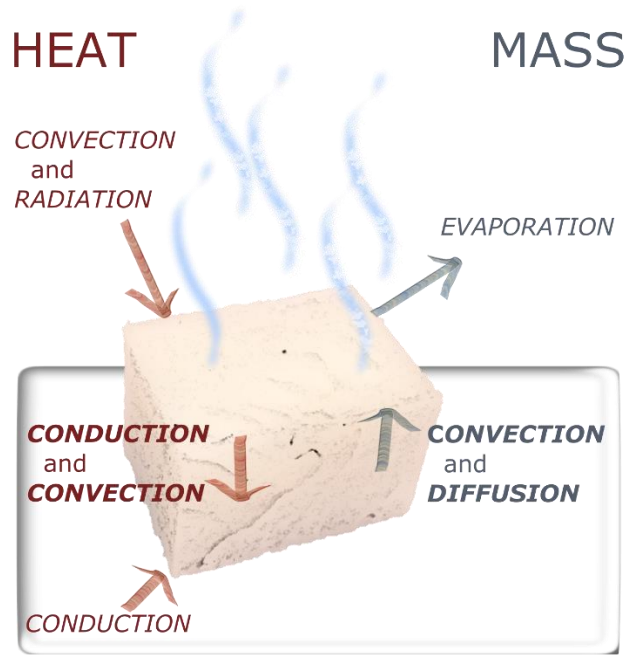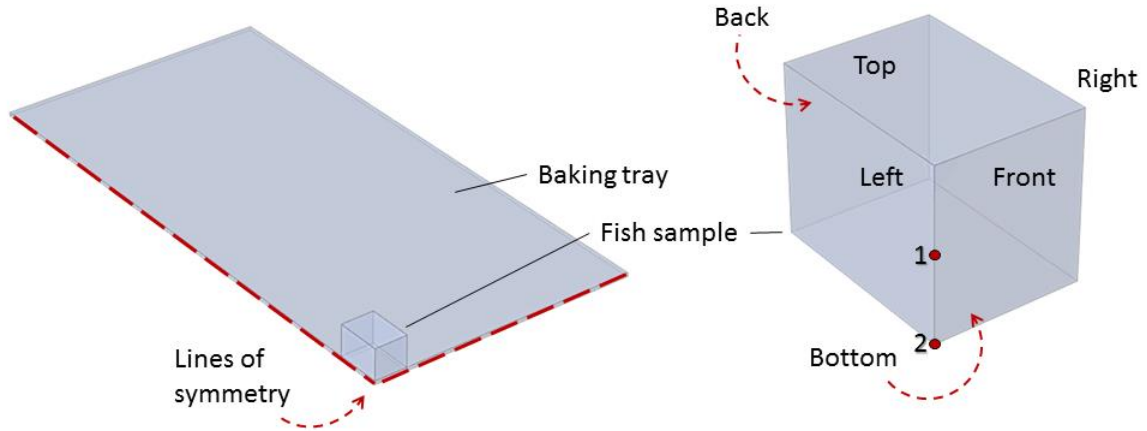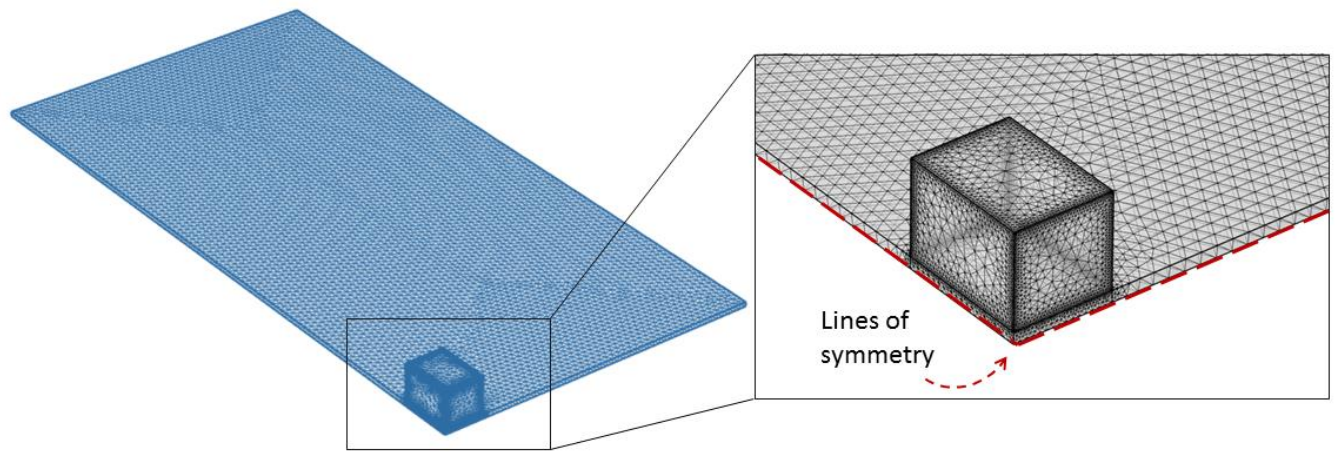537     backbone of Baltic cod (*Gadus morhua*). *Food hydrocolloids*, 24(4), 325-329.

**Figure 1. The heat and mass transport phenomena occurring during baking of small samples of cod fish on a baking plate in a convection oven.**

**Figure 2. The model geometry used in the model prediction.** Points 1 and 2 indicate the core and bottom surface positions for temperature validation.

**Figure 3. The meshing of the fish sample and baking tray used in the model prediction.**
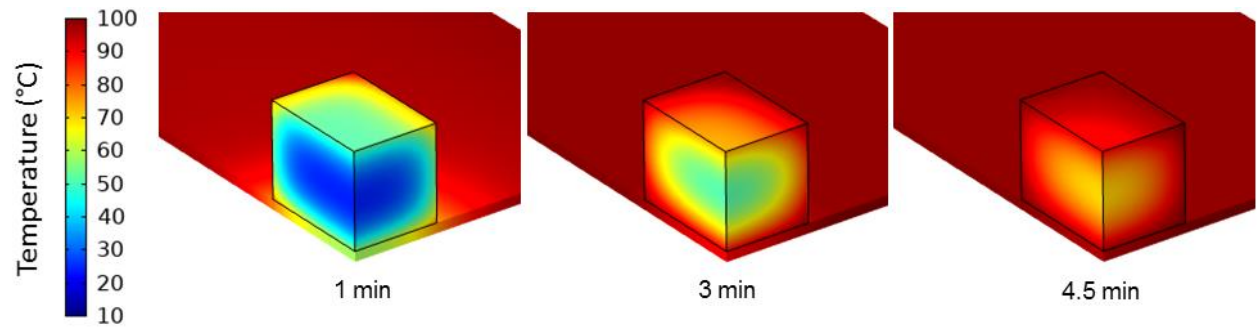
**Figure 4. Predicted temperature profiles of a cod sample (13.4x33.4x24.2 mm) and baking tray during cooking.** The reader is referred to the online version of this article for color.
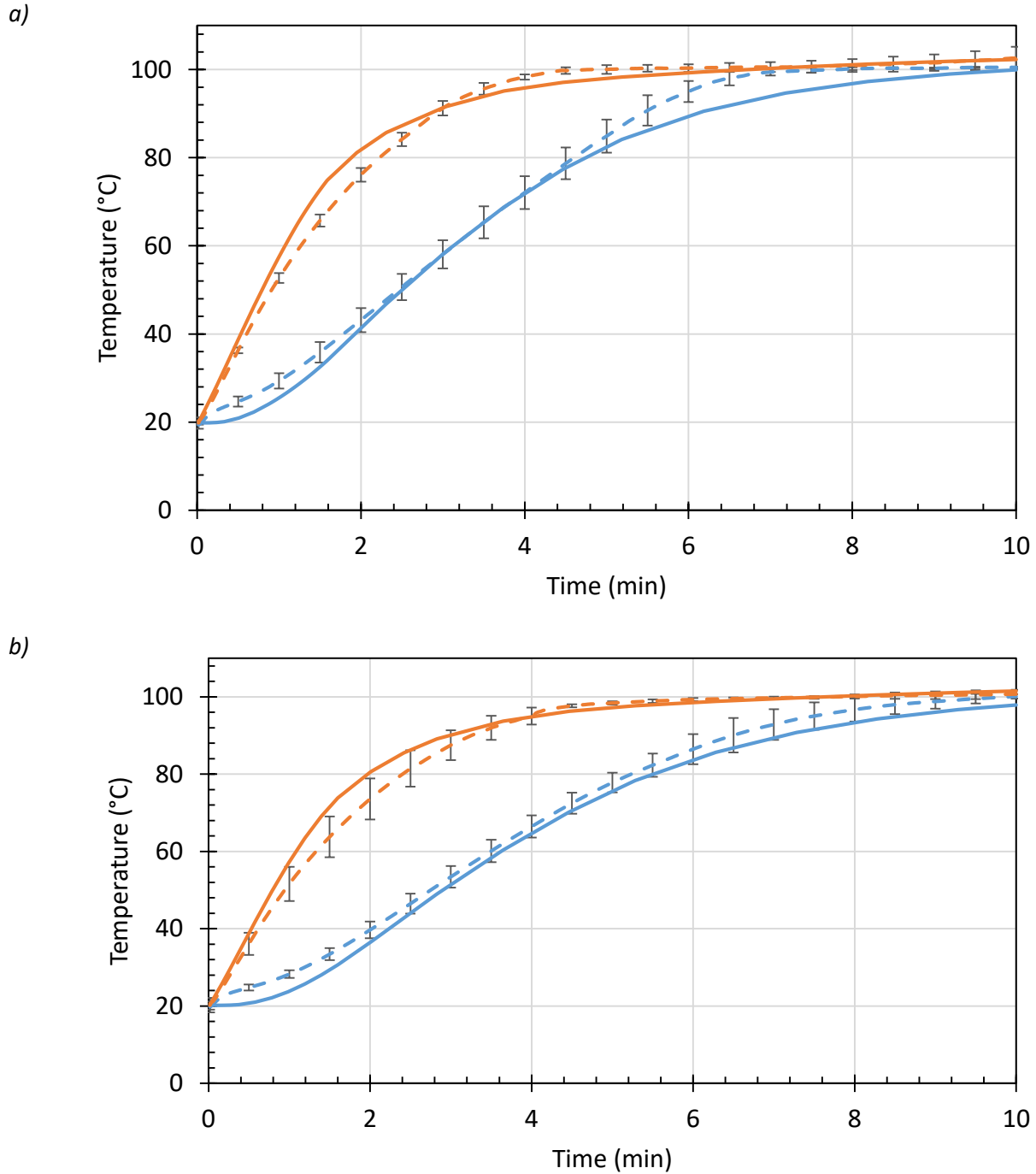
**Figure 5. Measured (±SD) and predicted temperature curves during cooking of cubes of cod fish on a baking tray in a convection oven.** *a)* Samples of height 11.5±0.50 mm (n=5); *b)* Samples of height 13.36±0.98 mm (n=6). Solid line: predicted; staggered line: measured. Blue: geometric core; orange: bottom surface. For clarity, the standard deviation is shown every 30 s. The reader is referred to the online version of this article for color.
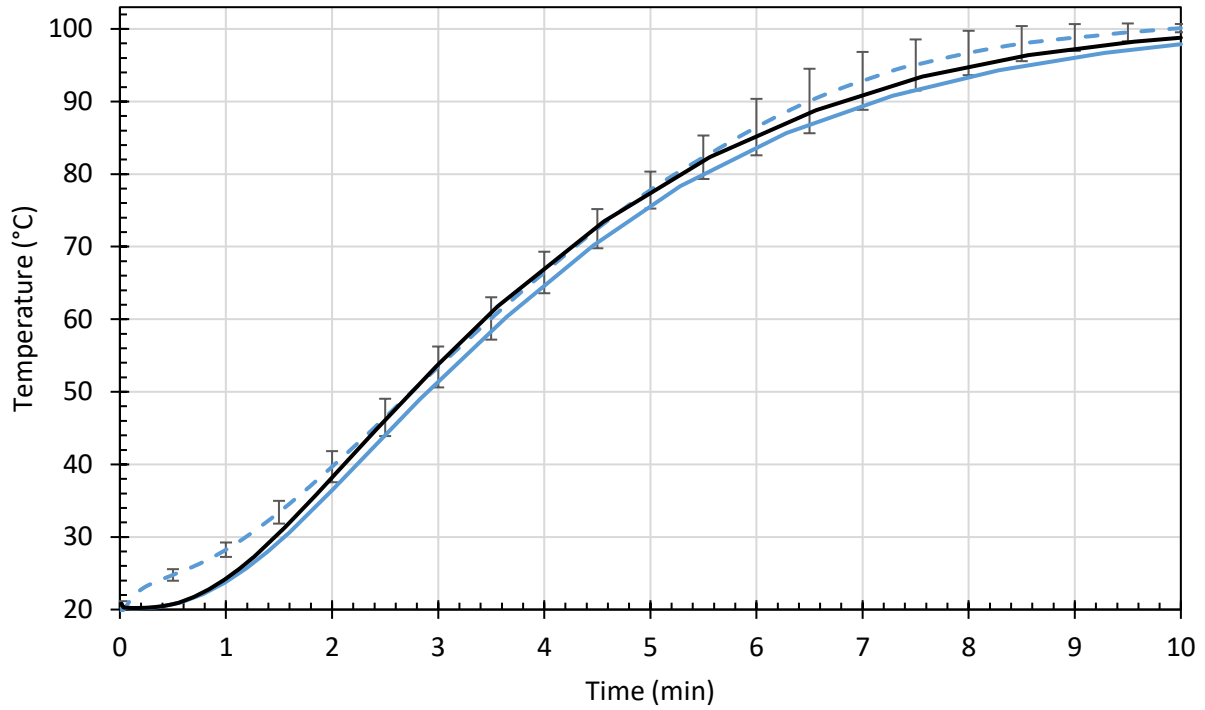
**Figure 6. Measured (staggered line, ±SD) and predicted (solid line, blue color) core temperature, and the effect of including the thermocouple (black color) in the model** for samples of height 13.36±0.98 mm (n=6). For clarity, the standard deviation is shown every 30 s. The reader is referred to the online version of this article for color.
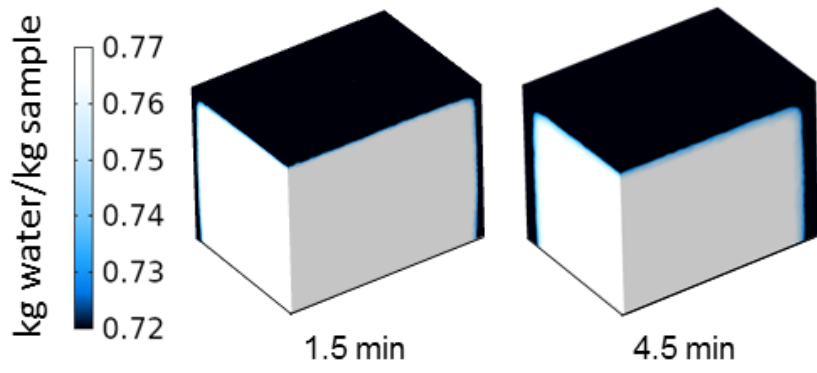
**Figure 7. Predicted water profiles of a cod sample (13.4x33.4x24.2 mm) after cooking for 1.5 and 4.5 minutes.** The reader is referred to the online version of this article for color.
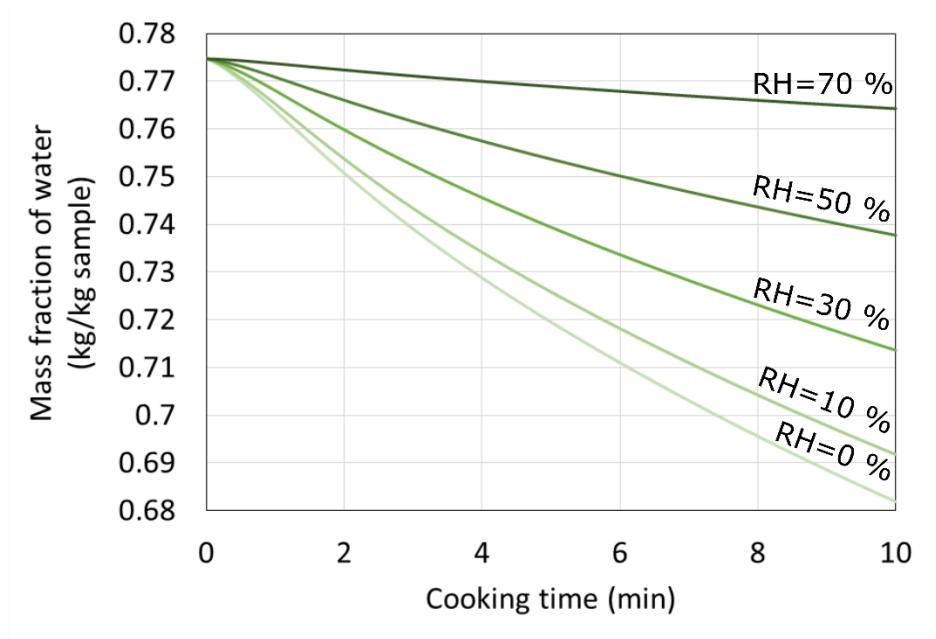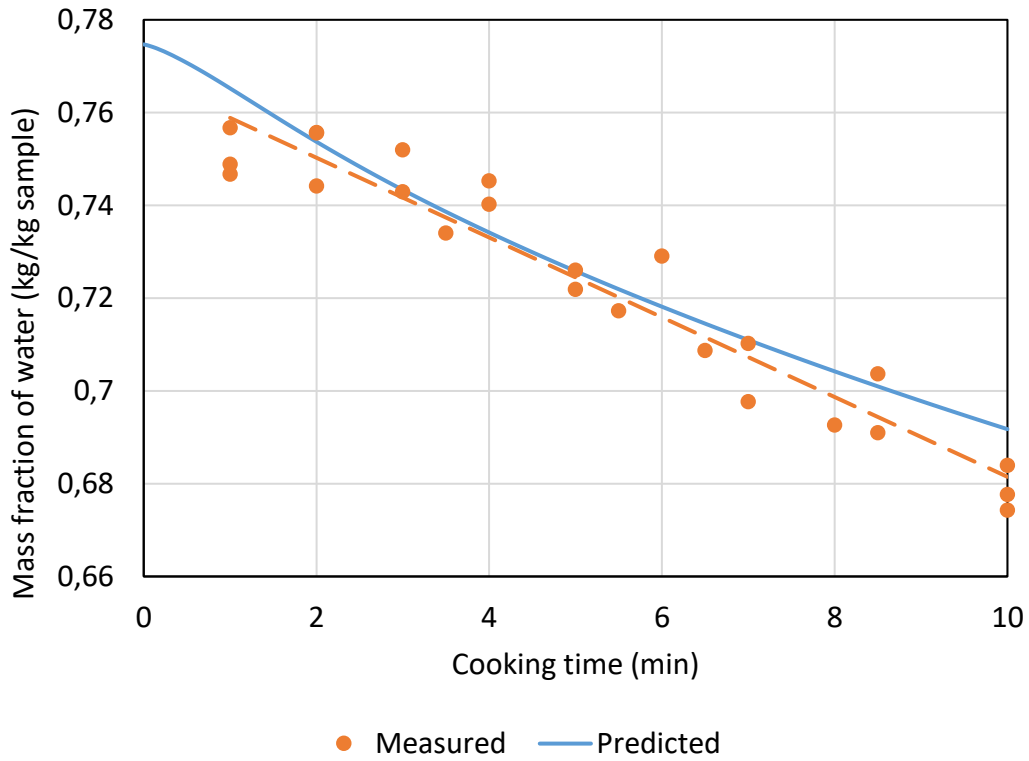
**Figure 8. Predicted average mass fraction of water in fish samples during cooking with 0, 10, 30, 50, and 70 % relative humidity (RH) in the oven.**

**Figure 9. Predicted (RH=10 %) and measured mass fraction of water in the fish sample and its change during cooking.** A trend line (staggered line, $R^2$=0.93) is included to emphasis the linear tendency of the decrease in the mass fraction of water with respect to cooking time.
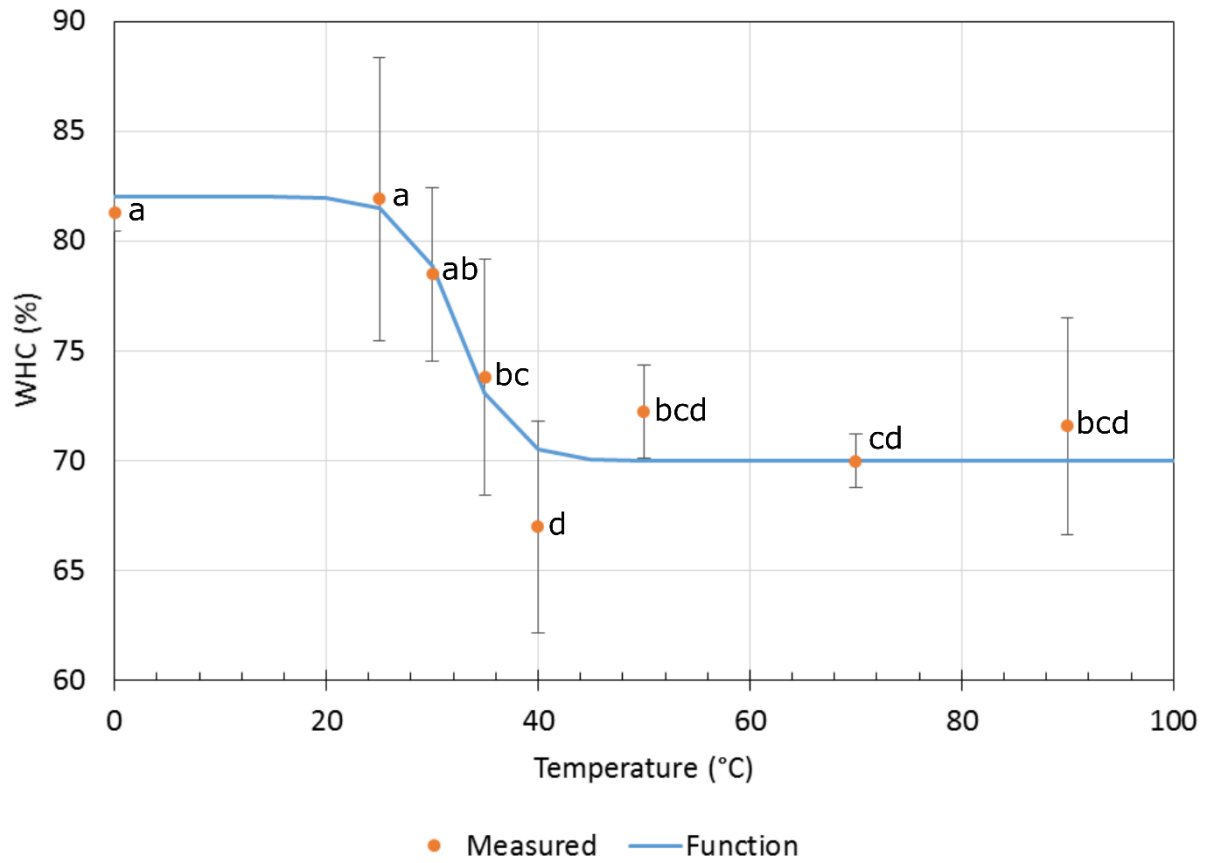
**Figure 10. The measured average water holding capacity (WHC; ±SD) of cod after cooking at 0-100 °C for 10 minutes (n=8), and the fitted sigmoidal function.** Measurement points not sharing a letter are significantly different.
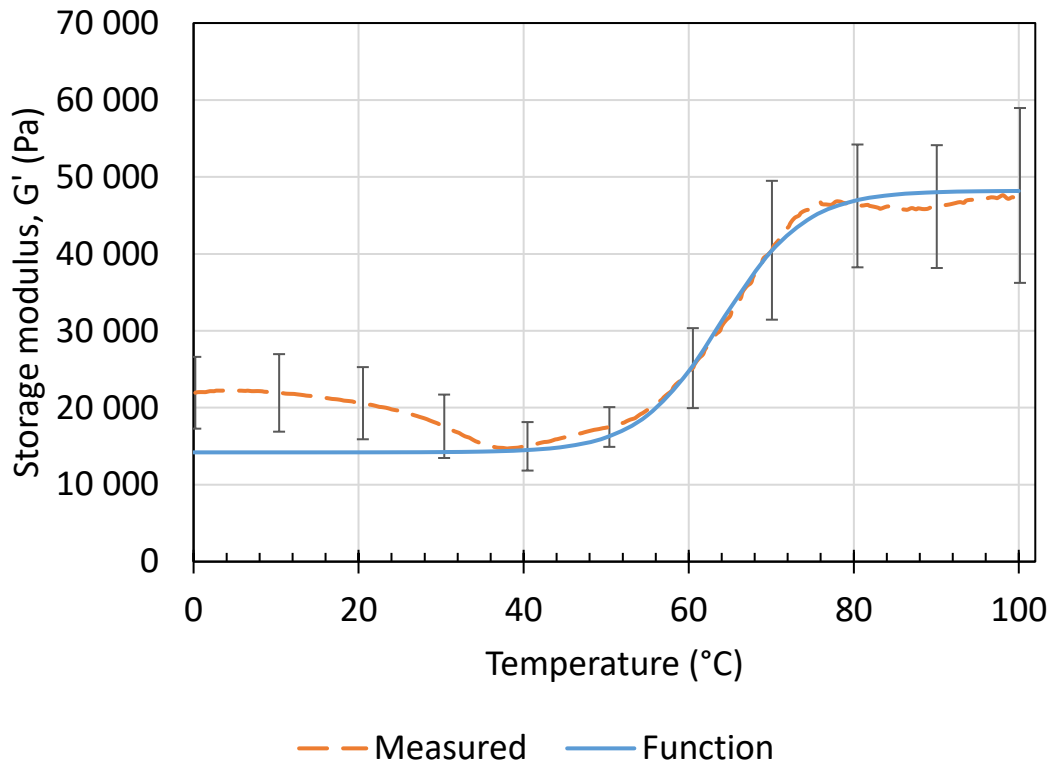
**Figure 11. The measured average storage modulus (±SD) of cod samples heated from 0-100 °C (n=9), plotted with the fitted sigmoidal function.** For clarity, standard deviation is included each 10 °C.
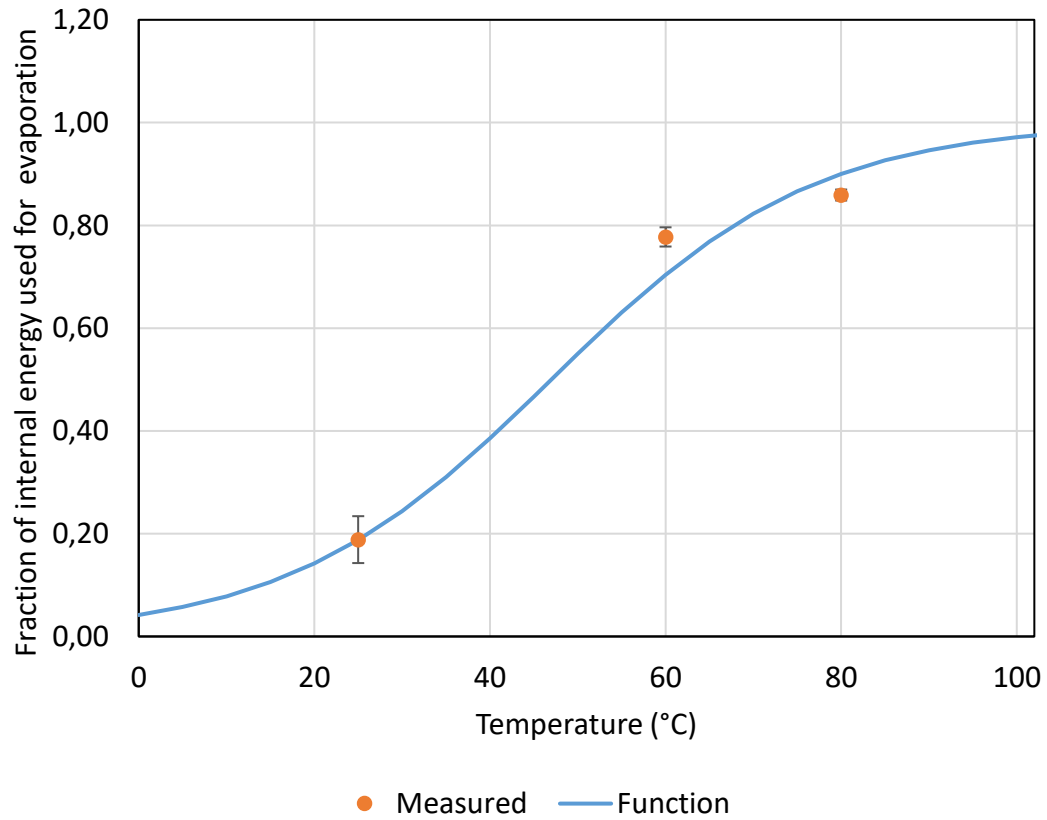
**Figure 12. The measured (n=4, ±SD) fraction of internal energy used for evaporation at the sample surface, plotted against the average core temperature of the investigated time interval used for calculation (0-50 °C, 50-70 °C and 70-90 °C).** The data are plotted with the fitted sigmoidal function, $f_{evap}(T)$.

**Table 1. Input properties in the model.**

| Symbol | Property | Value/equation | Unit | Source |
|---|---|---|---|---|
| $\kappa$ | Permeability | $10^{-17}$ | m² | Based on property for meat; Datta (2006) |
| $\sigma$ | Stefan Boltzmann's constant | $5.676 \times (10^{-8})$ | W/(m² K⁴) | |
| $c$ | Concentration of water at t = i | $x_{wi}\left(\dfrac{\rho_{cod}}{M_w}\right)$ | mol/(m² s) | |
| $C_{air}$ | Mass fraction of water in the air (kg water/kg water at saturation) | 0.1 | - | Measured |
| $c_{p,cod}$ | Specific heat of the cod | 3650 | J/(kg K) | Skipnes, Østby, & Hendrickx (2007) |
| $c_{p,plate}$ | Specific heat capacity of the baking plate (20°C) | 500 | J/(kg K) | Köckher & co (2019) |
| $c_{p,w}$ | Specific heat of water (55 °C) | 4180 | J/(kg K) | Singh & Heldman (2014) |
| $D_w$ | Diffusion coefficient of water in cod | $4 \times 10^{-10}$ | m²/s | Swordfish: Valle & Nickerson (1968) Pork: Vestergaard, Risum, & Adler-Nissen (2005)[1] |
| $h_c$ | Convective heat transfer coefficient | 41 | W/(m² K) | Measured |
| $H_{evap}$ | Latent heat of evaporation | $2.3 \times 10^6$ | J/kg | |
| $h_{total}$ | Total heat transfer coefficient | 55 | W/(m² K) | Measured |
| $k_{cod}$ | Thermal conductivity of cod | 0.515 | W/ (m K) | Skipnes, et al. (2007) |
| $k_{plate}$ | Thermal conductivity of the baking plate (20°C) | 15 | W/ (m K) | Köckher & co (2019) |
| $T_{oven}$ | Average oven temperature | 146.8±2.85 | °C | Measured |
| $T_{wall}$ | Wall temperature of oven | 144 | °C | Measured |
| $\mu_w$ | Dynamic viscosity of water | $\left(2.414 \times 10^{-5} \times 10^{\left(\frac{247.8}{(T+273.15)-140}\right)}\right)$ | Pa s | Singh & Heldman (2014) |
| $\rho_{cod}$ | Density of cod | 1060 | kg/m³ | Skipnes, et al. (2007) |
| $\rho_{plate}$ | Density of the baking plate | 7900 | kg/m³ | Köckher & co (2019) |
| $\rho_w$ | Density of water (55 °C) | 986 | kg/m³ | Singh & Heldman (2014) |

---

[1] Valle & Nickerson (1968) studied drying of fresh swordfish at 55 °C, and Vestergaard, et al. (2005) studied salting of pork.